Int. J. Heat Mass Transfer. Vol. 20, pp. 331–340. Pergamon Press 1977. Printed in Great Britain

MASS-TRANSFER FACTORS FROM ACTUAL DRIVING FORCES FOR THE FLOW OF GASES THROUGH PACKED BEDS ($0.1 < Re < 100$)

THOMAS H. HSIUNG and GEORGE THODOS
Northwestern University, Evanston, IL 60201, U.S.A.

(*Received* 7 *July* 1975 *and in revised form* 24 *June* 1976)

Abstract—Concentration profiles of naphthalene vapor were measured in the flow of air through packed beds of naphthalene spheres dispersed in a matrix of inert beads of styrene divinylbenzene copolymer. These profiles permitted the establishment of average actual driving forces, $(\Delta p)_a$, used to obtain corresponding actual mass-transfer coefficients. Six different particle sizes ranging from 0.02480 to 0.2000 cm in diameter were used in a single reactor, 6.59 cm (2.59 in) in diameter.

A plot of j_d-factor vs Reynolds number obtained from the data of this study was found to be linear on log–log coordinates which can be expressed in equation form as, $j_d = 1.33/Re^{0.40}$ in the range investigated ($0.1 < Re < 100$). This relationship, which includes axial and radial dispersion contributions, differs from that of earlier studies in which the log-mean driving force, $(\Delta p)_m$, was assumed to apply. The information of this study has been applied to the tank-in-series model to produce the dependence of Peclet number of Reynolds number, needed for the establishment of the actual mixing factor, defined as $F = (\Delta p)_a/(\Delta p)_m$.

NOMENCLATURE

- a, specific surface area [cm^2/cm^3];
- c, concentration of transferable component [g-mol/cm^3];
- D_p, average particle size [cm];
- D_v, gas diffusivity [cm^2/s];
- E, pseudo-dispersion coefficient for axial and radial mixing [cm^2/s];
- E_a, axial dispersion coefficient [cm^2/s];
- F, axial mixing factor, $(\Delta p)_a/(\Delta p)_m$, equation (5);
- G, superficial mass velocity [g/s cm^2];
- j_d, mass-transfer factor, $(k_g p_{gf} M_m/G)(\mu/\rho D_v)_f^{2/3}$;
- k_g, actual mass-transfer coefficient [g-mol/s cm^2 atm];
- L, height of packed bed [cm];
- M_m, mean molecular weight of flowing gas;
- n, number of perfect mixers, equations (8) and (9);
- p, partial pressure of transferable component [atm];
- Pe, Peclet number, $D_p u/\varepsilon E$;
- p_{gf}, partial pressure of nontransferable component [atm];
- p_s, partial pressure of transferable component at saturated conditions [atm];
- Δp_i, inlet driving force [mm Hg];
- Δp_0, outlet driving force [mm Hg];
- $(\Delta p)_a$, actual driving force [atm];
- $(\Delta p)_m$, log-mean driving force [atm];
- r, rate of mass transfer [g-mol/s];
- R, driving force ratio, $\Delta p_i/\Delta p_0$, equation (8);
- Re, Reynolds number, $D_p G/\mu$;
- Sc, Schmidt group, $\mu/\rho D_v$;
- t, time;
- t_s, surface temperature [°C];
- T, absolute temperature [K];
- u, actual fluid velocity [cm/s];
- V, volume of bed [cm^3];
- y, naphthalene composition in air [mole fraction];
- y_0, naphthalene composition in air leaving [mole fraction];
- y_s, naphthalene composition in air at surface of active particles [mole fraction];
- z, height of bed [cm].

Greek symbols

- ε, void fraction;
- μ, absolute viscosity [g/cm s];
- π, average system pressure;
- ρ, absolute density of gas [g/cm^3];
- ρ_d, absolute density of diluent [g/cm^3];
- ρ_s, absolute density of naphthalene particles [g/cm^3].

DURING the last thirty years considerable experimental information has been reported in the literature to describe the mass-transfer behaviour between gases and solid particles in packed beds. In this connection, mass-transfer studies have been reported for a number of gas–solid systems over extended ranges of Reynolds number. In 1943, Gamson *et al.* [1] presented mass-transfer data for the evaporation of water from the surface of Celite spheres into an air stream flowing through the voids of packed beds of these particles. Their experimental results were correlated in terms of j_d, the mass-transfer factor, against Re, the particle Reynolds number. Since their pioneering work, additional information has appeared in the literature to include other systems. In 1953, Chu *et al.* [2] presented mass-transfer data for the naphthalene–air system in both packed and fluidized beds. Further studies aimed to extend our knowledge in this field are reported in the literature [3–7] for gas–solid systems.

All these experimental studies have used log-mean driving forces for the calculation of mass-transfer coefficients and have neglected the contributions due to axial and radial dispersions. At high Reynolds numbers, their contribution is small, however, in the low Reynolds region these effects cannot be ignored. In 1953, Danckwerts [8], using a material balance over a differential length of packed bed, dz, and assuming Fick's law of diffusion to be valid over this distance, showed that the following relationship applies:

$$E_a \frac{\partial^2 c}{\partial z^2} - u\frac{\partial c}{\partial z} + \frac{\partial c}{\partial t} = 0 \qquad (1)$$

where c = concentration of the transferable component, E_a = axial dispersion coefficient, and u = fluid velocity through the interstices of the packed bed.

Carberry and Bretton [9] and Epstein [10] discuss the magnitude of the corrections necessary for axial dispersion in packed beds. For a number of practical cases, it was found that the axial-mixing effect was very small, however, for shallow beds this contribution could not be ignored. This mixing effect also becomes significant for flow conditions corresponding to low Reynolds numbers. The presence of axial dispersion has been rationalized in the past by considering a fixed bed to consist of a number of perfect mixers in series. According to this concept, Epstein [10] introduces in the rate relationship, the axial mixing factor, F, as follows:

$$r = k_g a V F (\Delta p)_m \qquad (2)$$

where $(\Delta p)_m$ is the log-mean driving force.

Mass transfer in packed beds is essentially a diffusional phenomenon through a stagnant film in the high Reynolds region where the contributions of axial and radial dispersion are relatively unimportant. With decreasing Reynolds numbers, both axial and radial dispersion contributions become significant and therefore these effects no longer can be neglected. At very low Reynolds numbers, $Re < 1.0$, these dispersion effects become molecular in nature and consequently molecular diffusion dominates the mechanism of mass transfer. To account properly for them, it becomes necessary to design an experimental procedure which will permit the separation of the diffusional effects from the coexisting dispersion contributions. Information relevant to this subject can be obtained by measuring actual driving forces existing within a packed bed. The departure of the measured driving force from the corresponding log-mean value should produce information that reflects in a combined manner the contribution of axial and radial dispersion effects associated with the physical transport of mass across a stagnant film.

EXPERIMENTAL EQUIPMENT AND PROCEDURE

Mass-transfer studies were conducted for the naphthalene–air system. Essentially spherical particles of naphthalene were prepared by the method outlined by Kato *et al.* [5]. Their method utilizes a column of water, the upper section of which is heated externally with heating tape while the lower section is kept cold with a water bath. Naphthalene powder, introduced in the heated zone melted at 80°C, and upon stirring, was dispersed into small droplets that solidified upon settling through the cold region. These naphthalene particles were removed, air dried, and screened into size ranges of six groups. An optical microscope was used to establish the average particle size by examining a sample of 250–350 particles, selected randomly from each group. The average particle sizes associated with each of the six groups ranged from 0.02480 to 0.2000 cm. Using a water displacement technique, the apparent density of these naphthalene particles was measured and was found to vary from 1.034 to 1.061 g/cm^3. This density variation results from the inclusion of small air bubbles within the spheres in the course of their preparation.

In order to void saturated exit conditions of naphthalene vapors in the air flowing through the bed, it was found necessary to disperse the naphthalene particles within a matrix of inert spheres. Beads of styrene divinylbenzene copolymer were used as the inert diluent for these active spheres. These beads were subjected to an exhaustive series of tests to establish their response to possible naphthalene adsorption. It was found that naphthalene vapors would not adsorb nor desorb from these nonporous polystyrene beads after an initial exposure to naphthalene vapors. To further confirm the reliability of this polystyrene diluent, runs were conducted in which the same quantity of naphthalene was dispersed in different amounts of this diluent. For one of these series (D_p = 0.04895 cm), the ratio of diluent to active naphthalene spheres was varied from 20 to 70, using the same air flow rate. For these runs, essentially constant values of k_g resulted. The results of this series of runs appears in Tables 1 and 2 as runs B4, B5, and B6. From these results, it was concluded that polystyrene beads were an appropriate diluent and therefore were used throughout this study. In this context, it should be noted that Bar-Ilan and Resnick [3] also used polystyrene spheres as a diluent in their mass-transfer studies with naphthalene. Each size of naphthalene particles of this study was properly accommodated with polystyrene beads of the same size with which they were mixed in order to prepare the packed beds for investigation.

The experimental equipment used in this investigation is essentially of the same type employed by Wilkins and Thodos [11] and by Yoon and Thodos [12]. This equipment included a reactor, constructed of Lucite tubing, i.d. = 6.59 cm (2.59 in), 0.318 cm (1/8 in) thick, and 38.2 cm (15 in) in length. Figure 1 presents a schematic diagram of this experimental facility. The calming section of the reactor was fabricated from brass and included a screen and a bed of brass sphere, 0.95 cm (3/8 in) in diameter. This arrangement permitted a uniform velocity profile of approach to the stainless steel porous plate (1/16 in thick) which supported the packed bed.

The top of the closure was also fabricated of brass and accommodated two travelling thermocouple

Table 1. Experimental data for the naphthalene–air system in packed beds
Reactor: i.d. = 6.59 cm Diluent: Styrene divinylbenzene copolymer beads (ρ_d = 1.04 g/cm^3)

Run	π (mm)	t_s(°C)	Naphthalene* (g)	Diluent (g)	Bed height L(cm)	ε	$G \times 10^3$ (g/s cm^2)	$r \times 10^3$ [g mol/s]	Composition (mole fraction) $y_0 \times 10^3$	$y_s \times 10^3$	$(\Delta p)_a \times 10^8$ (atm)
D_p = 0.02480 cm (ρ_s = 1.060 g/cm^3)											
AA-1	751.4	22.27	0.3021	28.00	1.25	0.360	0.880	0.837	8.106	8.859	2.523
AA-2	753.5	21.25	0.3115	24.00	1.10	0.375	0.883	0.762	7.360	7.991	2.028
AA-3	753.1	22.00	0.3251	24.00	1.10	0.375	1.216	1.112	7.796	8.605	2.559
AA-4	752.4	21.59	0.3210	27.00	1.19	0.351	1.215	1.090	7.646	8.275	2.556
AA-5	752.5	22.06	0.3280	33.50	1.48	0.354	1.215	1.136	7.973	8.666	2.505
AA-6	751.5	22.99	0.2597	26.00	1.20	0.381	1.546	1.498	8.261	9.506	3.403
AA-7	753.6	21.71	0.3531	27.50	1.25	0.370	1.552	1.342	7.380	8.367	2.980
AA-8	752.4	22.40	0.3356	27.00	1.20	0.356	1.903	1.762	7.895	8.961	2.945
AA-9	751.6	21.84	0.3342	28.00	1.25	0.360	2.231	1.985	7.557	8.491	2.838
AA-10	751.6	22.39	0.4225	28.00	1.25	0.357	2.932	2.650	7.708	8.963	2.623
AA-11†	747.7	23.20	0.7598	40.00	0.90	0.369	1.691	3.749	9.323	9.752	2.571
AA-12†	747.8	23.37	0.7483	50.25	1.06	0.330	2.422	5.413	9.398	9.914	2.965
D_p = 0.03446 cm (ρ_s = 1.057 g/cm^3)											
A-1	752.5	22.33	0.5579	34.00	1.50	0.349	2.236	2.030	7.743	8.900	2.996
A-2	752.5	22.06	0.5591	34.00	1.50	0.349	3.416	3.081	7.270	8.665	3.466
A-3	751.5	21.22	1.0174	37.00	1.75	0.386	3.632	3.165	7.432	7.988	2.092
A-4	751.8	22.90	0.9756	41.05	1.90	0.375	4.967	4.890	8.393	9.420	2.609
A-5	752.6	22.27	0.6050	34.00	1.50	0.348	4.970	4.382	7.518	8.845	3.399
A-6	755.9	21.05	0.5654	37.00	1.75	0.393	3.461	2.744	6.763	7.809	3.048
A-7	756.1	21.23	0.5663	37.00	1.75	0.393	6.331	4.895	6.596	7.947	3.036
A-8	752.5	22.00	0.5625	35.00	1.59	0.368	3.444	2.951	7.303	8.522	3.426
A-9	752.3	22.35	0.5609	35.00	1.59	0.368	2.920	2.714	7.926	8.866	3.300
A-10	752.5	22.22	0.5592	35.00	1.59	0.378	4.926	4.916	7.334	8.804	3.661
A-11	752.5	22.37	0.5632	35.00	1.70	0.409	7.916	6.902	7.435	8.934	3.609
D_p = 0.04895 cm (ρ_s = 1.061 g/cm^3)											
B-1	745.0	23.72	1.3811	54.30	2.65	0.408	4.899	5.384	9.370	10.30	3.464
B-2	744.6	23.45	1.1166	43.40	2.06	0.390	3.420	3.664	9.132	10.00	3.193
B-3	744.6	23.27	1.1402	43.80	2.06	0.385	6.261	6.224	8.480	9.815	3.586
B-4	744.6	23.63	1.1800	83.35	4.00	0.403	9.325	9.814	8.971	10.18	3.955
B-5	744.6	22.51	1.1949	24.25	1.15	0.375	9.328	8.532	7.799	9.154	3.325
B-6	739.4	22.18	1.0230	44.90	2.06	0.371	9.310	8.333	7.631	8.925	3.820
B-7	756.0	20.01	1.0087	50.00	2.31	0.376	3.464	2.568	6.323	7.041	2.477
B-8	756.1	20.36	1.0000	50.00	2.31	0.376	6.337	4.572	6.153	7.290	2.959
B-9	752.6	20.55	1.0610	50.00	2.40	0.399	12.60	8.728	5.905	7.428	3.902
B-10	752.6	22.64	1.0907	37.00	1.75	0.385	12.53	10.44	7.108	9.172	3.379
B-11	733.6	23.55	1.1340	27.00	1.25	0.364	4.870	4.891	8.650	10.29	3.872
B-12	752.5	22.50	0.8142	44.70	2.07	0.378	3.614	3.033	7.158	9.049	4.085
D_p = 0.0720 cm (ρ_s = 1.054 g/cm^3)											
C-1	744.9	22.92	1.3476	54.45	2.54	0.379	3.423	3.258	8.115	9.525	4.126
C-2	744.9	22.55	1.1400	54.95	2.54	0.376	14.09	10.63	6.431	9.187	5.229
C-3	739.4	21.79	1.0364	44.85	2.06	0.372	9.313	5.627	5.153	8.588	5.300
C-4	739.4	22.13	1.3386	74.80	3.49	0.384	9.310	6.255	5.728	8.881	5.184
C-5	739.4	22.25	1.3495	46.40	2.06	0.344	14.06	10.43	6.326	8.986	4.756
C-6	752.3	23.20	1.5510	45.00	2.00	0.342	3.441	3.347	8.298	9.694	3.454
C-7	752.4	22.80	1.5820	45.00	2.15	0.388	9.375	7.415	6.747	9.319	4.296
C-8	752.4	22.92	1.5800	45.00	2.15	0.395	7.911	6.569	7.082	9.430	3.928
C-9	737.5	19.39	1.5841	45.00	2.10	0.373	6.972	4.786	5.855	6.970	2.860
C-10	745.0	20.69	1.3670	26.40	1.23	0.362	12.45	7.010	4.801	7.645	4.227
C-11	745.0	21.30	1.4798	92.30	4.29	0.382	12.45	7.411	5.076	8.122	4.662
C-12	745.0	22.25	1.4058	54.95	2.54	0.373	4.926	3.764	6.519	8.918	4.301
D_p = 0.1073 cm (ρ_s = 1.054 g/cm^3)											
D-1	758.6	20.66	4.4515	54.00	2.70	0.389	9.443	7.368	6.656	7.487	2.451
D-2	756.0	19.50	4.4615	54.00	2.85	0.421	12.61	8.693	5.882	6.692	2.490
D-3	758.7	20.80	4.5383	55.50	2.90	0.415	15.69	12.01	6.527	7.590	2.449
D-4	758.8	20.78	4.4515	54.00	2.70	0.389	20.96	15.79	6.422	7.573	3.025
D-5	756.2	19.67	4.4615	54.00	2.80	0.410	20.96	13.97	5.682	6.805	2.912
D-6	759.0	20.29	8.0070	67.00	3.50	0.395	26.13	20.15	6.578	7.223	2.233
D-7	759.0	20.99	5.0090	55.50	2.95	0.421	31.44	22.45	6.092	7.731	3.675
D-8	759.1	20.80	4.5383	55.50	2.95	0.425	38.91	26.02	5.704	7.585	3.706
D_p = 0.2000 cm (ρ_s = 1.034 g/cm^3)											
H-1	755.8	21.34	33.50	0	1.50	0.365	29.61	27.90	8.037	8.037	1.503
H-2	755.9	21.41	28.50	0	1.25	0.352	48.29	43.21	7.631	8.092	2.086
H-3	755.9	21.51	28.50	0	1.30	0.376	67.81	58.16	7.313	8.171	3.121
H-4	752.3	22.60	20.10	0	0.96	0.405	38.58	36.75	8.124	9.138	3.249
H-5	752.5	22.65	24.50	0	1.10	0.367	58.34	57.29	8.375	9.183	3.182

π = Average system pressure; L = bed height; t_s = surface temperature; y_0 = naphthalene composition of air leaving [mole fraction]; y_s = naphthalene composition of air at surface of active particles [mole fraction].

*Initial weight of naphthalene [g].

†Size of reactor: i.d. = 9.37 cm (3.69 in).

Table 2. Calculated mass-transfer values for the naphthalene–air system

Run	adV (cm²)	Δp_i (mm)	Δp_0 (mm)	$R = \frac{\Delta p_i}{\Delta p_0}$	$(\Delta p)_m \times 10^5$ (atm)	F	$k_g \times 10^4$	j_d	cj_d	Re	n	Pe	Fcalc'd
$D_p = 0.02480$ cm ($\rho_s = 1.060$ g/cm³)													
AA-1	69.0	0.06657	0.00566	11.76	3.251	0.776	0.481	2.94	1.06	0.119	5.06	0.201	0.786
AA-2	71.1	0.06021	0.00482	12.50	2.884	0.703	0.528	3.22	1.21	0.120	3.78	0.170	0.754
AA-3	74.2	0.06483	0.00609	10.64	3.268	0.783	0.586	2.60	0.975	0.165	5.02	0.226	0.785
AA-4	72.3	0.06226	0.00473	13.16	2.983	0.870	0.590	2.61	0.916	0.165	9.48	0.395	0.784
AA-5	74.9	0.06521	0.00522	12.50	3.123	0.820	0.605	2.68	0.949	0.165	5.91	0.198	0.827
AA-6	59.3	0.07144	0.00936	7.63	4.018	0.847	0.742	2.58	0.984	0.209	6.27	0.259	0.835
AA-7	80.6	0.06305	0.00744	8.48	3.425	0.870	0.559	1.94	0.718	0.211	7.87	0.312	0.834
AA-8	76.6	0.06743	0.00802	8.40	3.672	0.802	0.781	2.21	0.787	0.258	5.00	0.221	0.834
AA-9	76.3	0.06382	0.00702	9.09	3.387	0.838	0.917	2.20	0.793	0.304	6.43	0.255	0.834
AA-10	96.4	0.06736	0.00943	8.33	3.679	0.713	1.086	1.99	0.710	0.398	3.30	0.131	0.856
AA-11*	173.4	0.07292	0.00321	22.73	2.935	0.876	0.841	2.66	0.982	0.229	12.02	0.662	0.687
AA-12*	170.8	0.07413	0.00385	19.23	3.128	0.948	1.069	2.36	0.779	0.327	27.97	1.31	0.760
$D_p = 0.03446$ cm ($\rho_s = 1.057$ g/cm³)													
A-1	91.9	0.06697	0.00871	7.69	3.759	0.797	0.737	1.78	0.621	0.421	4.67	0.214	0.841
A-2	92.1	0.06521	0.01050	6.21	3.943	0.879	0.965	1.44	0.503	0.681	7.26	0.333	0.866
A-3	167.6	0.06003	0.00420	14.29	2.764	0.757	0.903	1.34	0.516	0.681	4.99	0.197	0.841
A-4	160.7	0.07081	0.00772	9.17	3.743	0.697	1.166	1.26	0.473	0.935	3.24	0.117	0.883
A-5	99.4	0.06657	0.00999	6.67	3.925	0.866	1.297	1.41	0.491	0.939	6.75	0.310	0.874
A-6	93.2	0.05903	0.00791	7.46	3.346	0.911	0.966	1.51	0.593	0.654	10.91	0.430	0.881
A-7	93.3	0.06009	0.01022	5.88	3.702	0.820	1.728	1.48	0.582	1.196	4.60	0.181	0.904
A-8	92.7	0.06413	0.00917	6.99	3.720	0.921	0.929	1.45	0.534	0.650	12.04	0.522	0.873
A-9	92.4	0.06670	0.00707	9.43	3.496	0.944	0.890	1.64	0.604	0.550	19.63	0.851	0.845
A-10	92.1	0.06625	0.01106	5.99	4.059	0.902	1.264	1.38	0.522	0.929	8.86	0.384	0.887
A-11	92.8	0.06723	0.01116	5.95	4.125	0.875	2.061	1.40	0.573	1.492	6.81	0.276	0.905
$D_p = 0.04895$ cm ($\rho_s = 1.061$ g/cm³)													
B-1	159.6	0.07671	0.00690	11.11	3.815	0.908	0.974	1.06	0.432	1.31	12.69	0.469	0.881
B-2	129.0	0.07472	0.00650	11.41	3.674	0.869	0.890	1.39	0.542	0.913	8.87	0.421	0.835
B-3	131.7	0.07342	0.00999	7.35	4.184	0.857	1.318	1.12	0.431	1.67	6.63	0.315	0.879
B-4	136.3	0.07582	0.00902	8.40	4.128	0.958	1.821	1.04	0.419	2.49	24.84	0.608	0.938
B-5	138.0	0.06816	0.01009	6.76	4.001	0.831	1.859	1.06	0.398	2.50	5.33	0.454	0.814
B-6	118.2	0.06599	0.00957	6.90	3.843	0.994	1.845	1.05	0.390	2.49	153.9	7.30	0.892
B-7	116.5	0.05323	0.00543	9.80	2.755	0.899	0.890	1.39	0.523	0.932	10.89	0.462	0.861
B-8	115.5	0.05512	0.00860	6.41	3.295	0.898	1.338	1.14	0.429	1.70	8.80	0.373	0.899
B-9	122.6	0.05617	0.01151	4.38	3.914	0.997	1.824	0.916	0.365	3.39	239.5	9.77	0.933
B-10	126.0	0.06903	0.01553	5.88	4.250	0.795	2.452	1.05	0.404	3.35	4.00	0.224	0.891
B-11	131.0	0.07545	0.01200	6.29	4.539	0.853	0.949	1.02	0.371	1.23	5.92	0.464	0.809
B-12	94.1	0.06809	0.01423	4.79	4.529	0.902	0.789	1.18	0.446	0.967	7.75	0.367	0.893
$D_p = 0.0726$ cm ($\rho_s = 1.054$ g/cm³)													
C-1	105.7	0.07095	0.01050	6.76	4.163	0.991	0.731	1.140	0.432	1.36	107.2	6.15	0.855
C-2	108.7	0.06843	0.02053	3.33	5.475	0.955	2.044	0.708	0.266	5.59	13.05	0.746	0.931
C-3	81.3	0.06350	0.02540	2.50	5.470	0.969	1.305	0.742	0.276	3.70	14.54	1.02	0.929
C-4	105.0	0.06566	0.02331	2.82	5.383	0.963	1.149	0.653	0.251	3.70	13.97	0.581	0.952
C-5	105.8	0.06644	0.01967	3.38	5.054	0.941	2.073	0.780	0.268	5.58	10.06	0.708	0.915
C-6	121.6	0.07292	0.01050	6.94	4.238	0.815	0.797	1.250	0.428	1.36	4.89	0.355	0.817
C-7	119.8	0.07012	0.01935	3.62	5.188	0.828	1.441	0.828	0.321	3.72	3.51	0.237	0.906
C-8	123.9	0.07095	0.01767	4.02	5.042	0.779	1.350	0.919	0.363	3.14	2.90	0.196	0.895
C-9	124.2	0.05003	0.00800	6.25	3.017	0.948	1.347	0.993	0.370	2.79	17.21	1.190	0.857
C-10	107.2	0.05696	0.02119	2.69	4.760	0.888	1.547	0.663	0.240	4.96	4.25	0.501	0.902
C-11	116.0	0.06050	0.02269	2.68	5.073	0.919	1.371	0.587	0.224	4.95	5.89	0.199	0.971
C-12	110.2	0.06644	0.01787	3.72	4.865	0.884	0.794	0.860	0.321	1.96	5.42	0.310	0.909
$D_p = 0.1073$ cm ($\rho_s = 1.054$ g/cm³)													
D-1	236.2	0.05679	0.00630	9.01	3.022	0.811	1.273	0.732	0.285	5.56	5.42	0.431	0.832
D-2	236.7	0.05059	0.00621	8.26	2.770	0.899	1.475	0.633	0.266	7.44	10.05	0.757	0.852
D-3	240.8	0.05758	0.00806	7.14	3.314	0.739	2.036	0.705	0.293	9.24	3.41	0.252	0.872
D-4	236.2	0.05747	0.00874	6.58	3.403	0.889	2.210	0.573	0.223	12.4	8.13	0.646	0.877
D-5	236.7	0.05145	0.00849	6.06	3.125	0.924	2.050	0.529	0.217	12.4	11.48	0.880	0.886
D-6	424.8	0.05474	0.00482	11.36	2.707	0.825	2.127	0.442	0.175	15.4	6.52	0.400	0.883
D-7	265.7	0.05868	0.01244	4.72	3.922	0.937	2.299	0.397	0.167	18.5	12.05	0.876	0.925
D-8	240.8	0.05758	0.01428	4.03	4.082	0.907	2.916	0.407	0.173	22.9	7.26	0.528	0.931
$D_p = 0.2000$ cm ($\rho_s = 1.034$ g/cm³)													
H-1	972.0	0.06074	0	—	—	—	1.910	0.349	0.127	32.5	—	—	—
H-2	826.9	0.06117	0.00349	17.54	2.651	0.787	2.505	0.281	0.0989	52.9	6.22	1.99	0.535
H-3	826.9	0.06177	0.00649	9.52	3.228	0.967	2.253	0.180	0.0677	74.3	33.76	10.39	0.652
H-4	583.0	0.06112	0.00678	9.01	3.251	0.999	1.940	0.271	0.108	42.2	1065	443.8	0.659
H-5	710.8	0.06960	0.00612	11.36	3.140	0.933	2.364	0.218	0.0800	63.8	17.65	6.42	0.564

k_g = g-mol/s cm² atm.
*Size of reactor: i.d. = 9.37 cm (3.69 in).

probes and a sample probe that could be moved up and down for the withdrawal of air samples from different bed heights. This sampling probe was provided, at the tip inlet, with two crossed layers of 100-mesh stainless steel screen to prevent any solid carry-over. Each thermocouple probe carried a single copper–constantan thermocouple. One thermocouple measured the temperature of the air above the bed while the other was surrounded with a solid bead of naphthalene. This bead was prepared by melting naphthalene on the thermocouple junction which was offset to be near the surface of this bead. The temperature measured with this thermocouple was assumed to be the surface temperature of the naphthalene particles in the packed bed.

Packed beds of naphthalene particles and polystyrene beads were prepared by thoroughly mixing

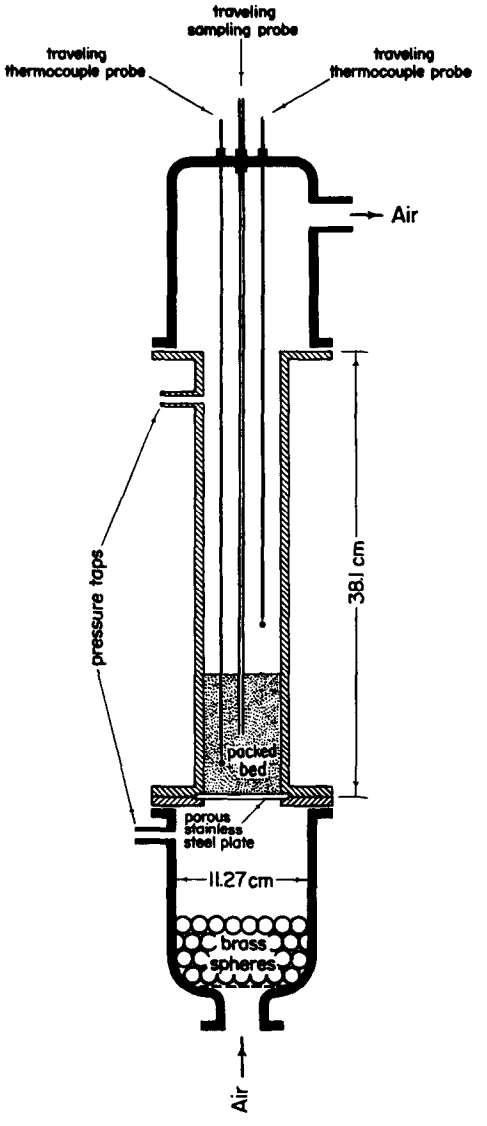

FIG. 1. Schematic diagram of experimental unit.

them together in the appropriate proportions. The dilution ratio, grams of polystyrene/gram of naphthalene was varied from zero to 100. In the course of a run, a gas sample was continuously withdrawn from the sampling probe. The position of the sampling probe in the course of a run was varied to traverse the entire height of the bed. The withdrawn sample was first passed through a solenoid sampling valve and was then introduced into a hydrocarbon analyzer of the flame ionization type (Beckman, Model 109A) using nitrogen as the carrier gas. This instrument was first calibrated by obtaining the response of air samples saturated with naphthalene vapors. These samples were prepared by passing air slowly through a bed of naphthalene particles (height = 22 cm). In order to ascertain saturated conditions, the flow rate of air through the naphthalene particles was slowly decreased until the instrument response became constant. For these conditions, the naphthalene content of the air was also checked with a material balance obtained by the weight loss of naphthalene. The instrument response corresponding to the saturation concentration of naphthalene in the air samples at the temperature of the system permitted the calibration of the hydrocarbon analyzer.

To avoid adsorption of naphthalene vapors on the walls of the sampling lines, all sampling lines leading to the analyzer were heated with electric-tape. The signal from the analyzer was transmitted to a recorder and the resulting response curve was integrated to obtain the naphthalene content of the air samples. This approach permitted the establishment of the concentration profile of naphthalene in air for each run. Altogether, 60 runs were completed using the six groups of particle sizes in a single reactor (i.d. = 6.59 cm). The experimental data resulting from this study are summarized in Table 1.

ANALYSIS OF EXPERIMENTAL DATA

The concentration of naphthalene vapor at the surface of the particles must be in equilibrium at the temperature of the solid. For solid naphthalene, the vapor pressure relationship of Gil'denblat *et al.* [13],

$$\log_{10} p_s(\text{mm}) = 11.424 - \frac{3722.5}{T,^\circ\text{K}} \quad (16^\circ\text{C} < t < 50^\circ\text{C}) \quad (3)$$

was used. Equation (3) produces values that are in close agreement to the vapor pressure values resulting from the relationship, $\log_{10} p_s(\text{mm}) = 11.450 - 3729.3/T^\circ\text{K}$ presented in the International Critical Tables [14] and used by Chu *et al.* [2]. A typical normalized partial pressure profile for naphthalene vapors is presented in Fig. 2 for run A5 which lasted 12 min. The duration of each run was monitored to be approximately 15 min, in order to ensure that the change of the average particle size did not exceed a variation of more than 5%. Relationships comparable to Fig. 2, were obtained for all the other runs. These relationships have been graphically integrated to establish the actual driving force, $(\Delta p)_a$, needed for the calculation of actual mass-transfer coefficients.

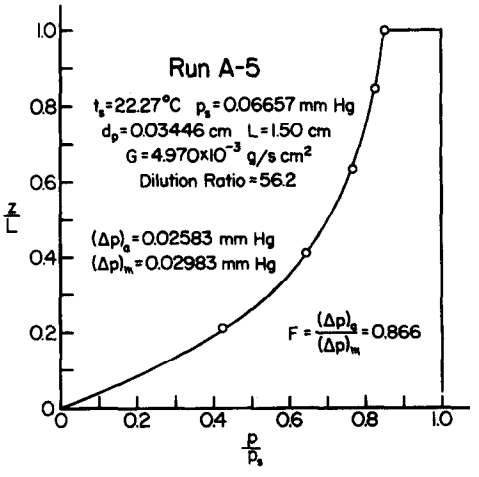

FIG. 2. Typical normalized partial pressure profile of naphthalene.

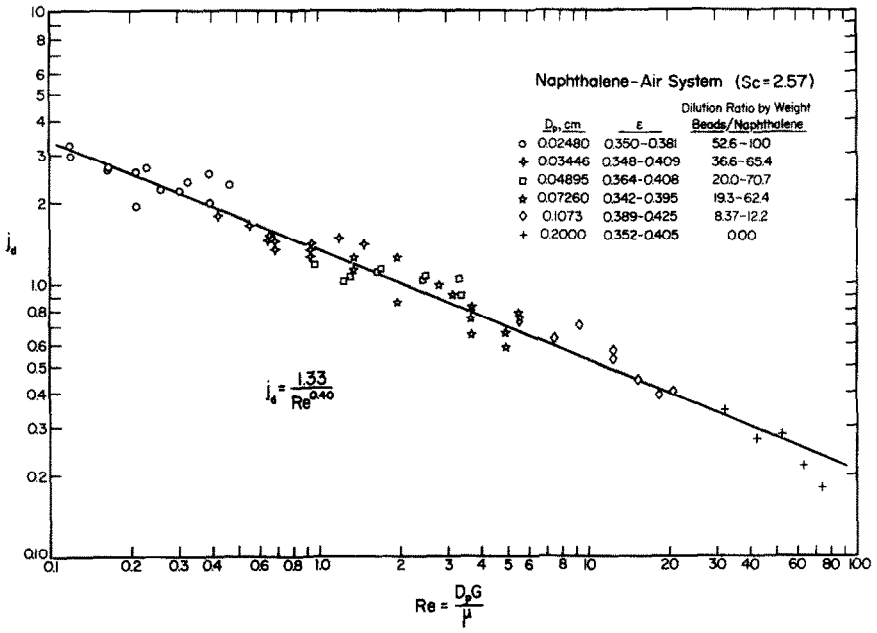

FIG. 3. Relationship between j_d and Re for packed beds established from driving forces involving actual concentration profiles.

Actual partial pressure profiles for naphthalene of the type presented in Fig. 2 should produce a log–mean partial pressure difference, if only plug flow conditions prevail within the packed bed. Deviations from this log–mean value signify the presence of axial and radial dispersion contributions. For run A5, the actual average driving force, $(\Delta p)_a = 0.02583$ mm (3.399×10^{-5} atm) while the corresponding log–mean value obtained from the end conditions is found to be $(\Delta p)_m = 0.02983$ mm (3.925×10^{-5} atm). The establishment of the actual measurement of $(\Delta p)_a$ allows the calculation of the true mass-transfer coefficient associated with the rate relationship,

$$r = k_g a V (\Delta p)_a. \tag{4}$$

When equation (4) is compared with equation (2), it follows that the actual mixing factor becomes,

$$F = \frac{(\Delta p)_a}{(\Delta p)_m}. \tag{5}$$

Values of F for the runs of this study are included in Tables 1 and 2 along with corresponding values $(\Delta p)_a$ and $(\Delta p)_m$ used to establish the values of the axial mixing factor, F, for all the 60 runs of this study.

Actual mass-transfer coefficients, k_g, calculated with equation (4), are presented in Table 2. These values were then used to calculate the corresponding mass-transfer factors, j_d, which are also presented in this table. For these calculations a Schmidt group value of $Sc = 2.57$ was used. This value is essentially constant over the temperature variation encountered for all runs and ranged from 19–24°C. This same value is reported by Chu *et al.* [2], Bar-Ilan and Resnick [3], Bradshaw and Bennett [15], and Kato *et al.* [5]. Values of j_d have been plotted vs Reynolds number to produce the linear relationship of Fig. 3. This relationship, resulting from the 60 runs of this study can be expressed in equation form as,

$$j_d = \frac{1.33}{Re^{0.40}} \quad (0.1 < Re < 100). \tag{6}$$

In order to establish a more generalized treatment [6] for these runs, the product εj_d has been related to the corresponding Reynolds number as shown in Fig. 4. The dependence of εj_d on Re can be best presented visually in an equation form as,

$$\varepsilon j_d = \frac{0.480}{Re^{0.39}} \quad (0.1 < Re < 100). \tag{7}$$

In this figure are included values of εj_d resulting from the data of Gamson *et al.* [1], DeAcetis and Thodos [4], Petrovic and Thodos [16] and Wilkins and Thodos [11]. Their values were corrected for axial dispersion using the approach outlined by Epstein [10] and a value of $Pe = 2$, suggested by Wilhelm [17]. The line resulting from these adjusted data lies slightly lower than that represented by equation (7). The deviation between these two correlations is undoubtedly due to insufficient correction necessary to account for the contribution of radial dispersion which is inherently present in equation (7). Equations (6) and (7) produce mass-transfer coefficients that take into account the coexisting axial and radial dispersion contributions in accordance with equation (4). For these relationships to be complete, it becomes necessary to establish F so that $(\Delta p)_a$ can be properly accounted for from the corresponding log–mean value, $(\Delta p)_m$, which is more directly discernible from the inlet and exhaust conditions of a packed bed.

Correlation of actual mixing factor, F

Values of the actual mixing factor, F, obtained from equation (5) include the contribution of both axial and

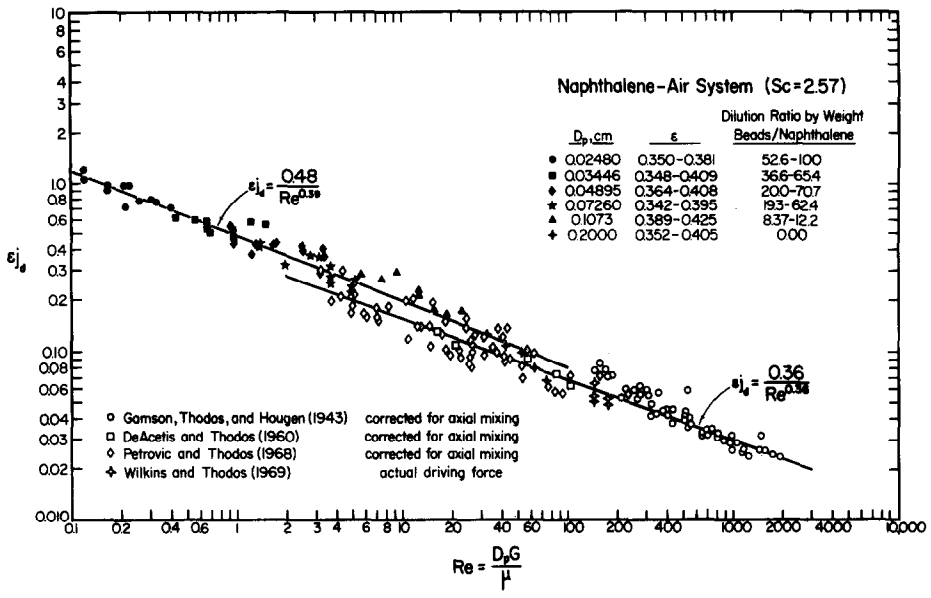

FIG. 4. Comparison of packed bed relationships between εj_d and Re resulting from actual driving forces and log-mean driving forces corrected for axial mixing.

radial dispersion under the flow conditions of the system. The analysis of these coexisting dispersion effects is not convenient to undertake in their combined form. In this connection, McHenry and Wilhelm [18] point out that in a packed bed, axial dispersion is approximately six times larger than the corresponding radial contribution. Largely, because of the dominant nature of the axial dispersion, it is reasonable to assume a pseudo-axial dispersion model that treats the smaller radial contribution in a manner similar to that outlined for axial dispersion. Using a model based on the number of perfect mixers in series for packed beds, Epstein [10] develops the axial mixing factor to be,

$$F = \frac{\ln R}{n(R^{1/n} - 1)} \tag{8}$$

where R = ratio of inlet to outlet driving potentials, and n = number of perfect mixing cells in series.

McHenry and Wilhelm [18] show that the number of perfect mixers in a fixed bed can be expressed as,

$$n = \frac{L}{D_p}\frac{Pe}{2} \tag{9}$$

where L = height of packed bed, D_p = average particle diameter and Pe = Peclet number, $D_p u/\varepsilon E$.

Wilhelm [17] summarizes experimental work available in the literature for both axial and radial dispersion in packed beds. Using a frequency response technique, McHenry and Wilhelm [18] obtained axial dispersion data for the gaseous systems hydrogen–nitrogen and ethylene–nitrogen and derived from these data, the dependence of the Peclet number on Reynolds number. Using the data of twenty-one runs for Reynolds numbers between 100 to 400, they conclude that the axial Peclet number is 1.88 ± 0.15. Aris and Amundson [19], using theoretical arguments, show that this axial Peclet number approaches, $Pe = 2$, as a limiting value, at high Reynolds numbers. In his review presentation, Wilhelm [17] indicates that for gaseous systems, molecular diffusion becomes increasingly significant with decreasing Reynolds numbers for $Re < 10$.

The combined axial–radial mixing factor, F, resulting from the measurements of the present investigation and the ratio of inlet to outlet driving potentials, R, permitted the evaluation of the number of mixing cells, n, using a trial-and-error procedure on equation (8). The values of n resulting from this treatment, enabled the calculation of the Peclet number, $Pe = D_p u/\varepsilon E$ through the involvement of equation (9). The resulting values of both n and Pe are also presented in Table 2. It should be pointed out that the calculated value of E associated with this Peclet number represents a pseudo-axial dispersion coefficient which includes, not only the axial, but also the simultaneous radial dispersion contribution. These calculated Peclet numbers which include both contributions have been related to their corresponding Reynolds numbers in Fig. 5. The high degree of sensitivity of n on F and R, as depicted by equation (8), reflects on the data of this figure which show a scatter, but indicate a dependence of Peclet number on Reynolds number that can be approximated through the relationship,

$$Pe = 0.34 Re^{0.22} \quad (0.1 < Re < 100). \tag{10}$$

This relationship has been used to produce Peclet numbers corresponding to the runs of this study and with equations (8) and (9), values of F were back-calculated. These calculated values are presented in Table 2 and can be compared with the corresponding values of F resulting from the actual driving force measurements. This comparison indicates that generally good agreement exists between values of F calculated using equations (10), (9), and (8) and the corresponding values obtained from the actual concentration profiles. The overall average deviation for all the runs was found to be 8.16%. Consequently, the

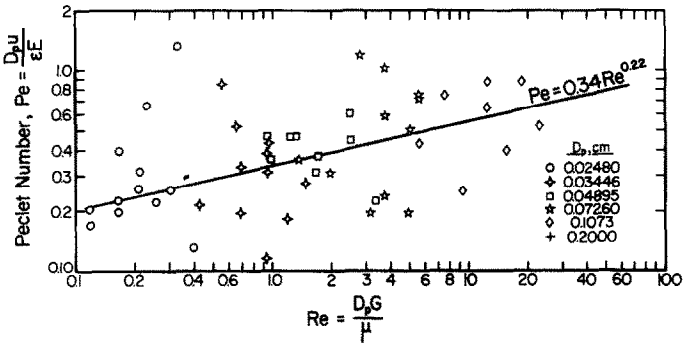

FIG. 5. Relationship between Peclet number and Reynolds number that includes the simultaneous axial and radial contributions present in the data of this study (naphthalene–air system, $Sc = 2.57$).

use of equation (10) justifies the calculation of a Peclet number which includes the combined axial and radial contribution inherently present in this mass-transfer operation.

STATISTICAL ANALYSIS OF DATA

The most important independent variables of this study are represented by the particle size and mass velocity. From the experimental results, the effect of active particle dilution and bed height have been shown to be insignificant. The experimental runs conducted in this study were essentially carried out in a random manner and therefore this approach introduces hardly any bias to the results. For each run, a new batch of naphthalene with the necessary inert particles was charged to minimize the effect of size shrinking and therefore the compromised particle size of the active particles is representative of the state prevalent under the specified flow conditions.

The results of the data presented in Fig. 3 exhibit a definite dependence between j_d and Re and in Fig. 4 between εj_d and Re. The relationships of these figures were visually established to produce the expressions represented by equations (6) and (7). However, a statistical approach using the original data becomes more convincing since the visual approach gives rise to expressions that are nearly the same as those resulting from the statistical arguments. When a linear regression analysis is applied to $\ln j_d$ and $\ln Re$, the following relationship results for Fig. 3:

$$j_d = \frac{1.33}{Re^{0.40}} \quad (0.70 < Re < 100). \tag{11}$$

Equation (11) is identical to equation (6) and is associated with a correlation coefficient of 0.984. For Fig. 4, the following functionality was found using the same approach:

$$\varepsilon j_d = \frac{0.499}{Re^{0.382}} \quad (0.1 < Re < 100) \tag{12}$$

with a correlation coefficient of 0.978. Figure 5 exhibits a scatter between the calculated values of the Peclet number, Pe, and Re, the particle Reynolds number. The visually established relationship of this figure is given by equation (10). However, the regression analysis approach involving $\ln Pe$ and $\ln Re$, produced the following dependence:

$$Pe = 0.379 Re^{0.22} \quad (0.1 < Re < 100). \tag{13}$$

As expected, equation (13) has a smaller correlation coefficient of 0.42. Equation (10) produces values for the Peclet number which are consistently lower than those resulting from equation (13), since the only difference between them exists in the coefficient terms 0.34 and 0.379.

The difference between equations (7) and (12) can best be represented by the variations at the boundaries of the Reynolds number range of interest as follows:

	εj_d	
	$Re = 0.1$	$Re = 100$
Equation (7)	1.18	0.0797
Equation (12)	1.20	0.0859
Deviation, %	1.7	7.2

as can be seen, the maximum deviation between these two equations is less than 7.2%.

CONCLUSIONS

Actual concentration profiles of naphthalene vapor, sublimed into air flowing through a packed bed of naphthalene spheres, were used to establish the prevailing actual mass-transfer coefficients, k_g, and the corresponding mass-transfer factors, j_d. For the sixty runs of this study which included the involvement of six different particle sizes, the Reynolds number was varied from 0.119 to 74.3. The functionality between actual mass transfer factor and particle Reynolds number was found to be $j_d = 1.33/Re^{0.40}$.

Graphical integration of these concentration profiles, yielded average driving forces which differed progressively from the corresponding log-mean values with decreasing Reynolds number. This difference results from the axial and radial dispersion effects which cannot be ignored with decreasing flow conditions. Both of these contributions have been accounted for

by the introduction of the axial mixing factor, F, needed for the establishment of the proper mass-transfer rate.

REFERENCES

1. B. W. Gamson, G. Thodos and O. A. Hougen, Heat, mass, and momentum transfer in the flow of gases through granular solids, *Trans. Am. Inst. Chem. Engrs* **39**, 1 (1943).
2. J. C. Chu, J. Kalil and W. A. Wetteroth, Mass transfer in a fluidized bed, *Chem. Engng Progr.* **49**, 141 (1953).
3. M. Bar-Ilan and W. Resnick, Gas phase mass transfer in fixed beds at low Reynolds numbers, *Ind. Engng Chem.* **49**, 313 (1957).
4. J. DeAcetis and G. Thodos, Mass and heat transfer in the flow of gases through spherical packings, *Ind. Engng Chem.* **52**, 1003 (1960).
5. K. Kato, K. Hiroshi and C. Y. Wen, Mass transfer in fixed and fluidized beds, *Chem. Engng Progr. Symp. Ser.* 105 **66**, 87 (1970).
6. J. T. L. McConnachie and G. Thodos, Transfer processes in the flow of gases through packed and distended beds of spheres, *A.I.Ch.E. Jl* **9**, 62 (1963).
7. A. Sen Gupta and G. Thodos, Direct analogy between mass and heat transfer to beds of spheres, *A.I.Ch.E. Jl* **9**, 751 (1963).
8. P. V. Danckwerts, Continuous flow systems: distribution of residence time, *Chem. Engng Sci.* **2**, 1 (1953).
9. J. J. Carberry and R. H. Bretton, Axial dispersion of mass in flow through fixed beds, *A.I.Ch.E. Jl* **4**, 367 (1958).
10. N. Epstein, Correction factor for axial mixing in packed beds, *Can. J. Chem. Engng* **36**, 210 (1958).
11. G. S. Wilkins and G. Thodos, Mass transfer driving forces in packed and fluidized beds, *A.I.Ch.E. Jl* **15**, 47 (1969).
12. P. Yoon and G. Thodos, Gas–solid fluidized systems: Average mass transfer potentials of shallow beds, *A.I.Ch.E. Jl* **19**, 625 (1973).
13. I. A. Gil'denblat, A. S. Furmanov and N. M. Zhavoronkov, Vapor pressure of crystalline naphthalene, *Zh. Prikl. Khim.* **33**, 246 (1960).
14. *International Critical Tables*, Vol. 3, p. 208. McGraw-Hill, New York (1928).
15. R. D. Bradshaw and C. O. Bennett, Fluid-particle mass transfer in a packed bed, *A.I.Ch.E. Jl* **7**, 48 (1961).
16. L. J. Petrovic and G. Thodos, Mass transfer in the flow of gases through packed beds, *Ind. Engng Chem. Fundamentals* **7**, 274 (1968).
17. R. H. Wilhelm, Progress towards the *a priori* design of chemical reactors, *Pure Appl. Chem.* **5**, 403 (1962).
18. K. W. McHenry and R. H. Wilhelm, Axial mixing of binary gas mixtures flowing in a random bed of spheres, *A.I.Ch.E. Jl* **3**, 87 (1957).
19. R. Aris and N. R. Amundson, Some remarks on longitudinal mixing or diffusion in fixed beds, *A.I.Ch.E. Jl* **3**, 280 (1957).

FACTEURS DE TRANSFERT MASSIQUE POUR L'ECOULEMENT DE GAZ A TRAVERS DES LITS FIXES ($0{,}1 < Re < 100$)

Résumé—On a mesuré des profils de concentration de vapeur de naphtalène dans l'air qui traverse des lits fixes de sphères de naphtalène dispersées dans une matrice inerte de copolymère de divinyl/benzene. Ces profils ont permis de dégager le paramètre $(\Delta p)_a$ utilisé pour obtenir les coefficients de transfert massique. Six tailles de particule entre 0,0248 et 0,2000 cm de diamètre sont utilisées dans un même réacteur de 6,59 cm de diamètre.

Un graphe de variation du facteur j_d en fonction du nombre de Reynolds est linéaire dans des coordonnées log–log, et il peut être exprimé par $j_d = 1{,}33/Re^{0,10}$ dans le domaine étudié ($0{,}1 < Re < 100$). Cette relation qui inclut les contributions des dispersions axiales et radiales, diffère de celle donnée dans des études antérieures dans laquelle est supposée intervenir la force motrice moyenne logarithmique $(\Delta p)_m$. L'information donnée par cette étude a été appliquée au modèle des réservoirs en série pour obtenir la dépendance entre nombre de Péclet et nombre de Reynolds, nécessaire pour établir le factor de mélange défini par $F = (\Delta p)_a/(\Delta p)_m$.

ERMITTLUNG DER STOFFÜBERGANGSFAKTOREN AUS DEN TATSÄCHLICHEN, TREIBENDEN KRÄFTEN FÜR DIE STRÖMUNG VON GASEN DURCH FESTBETTEN ($0{,}1 < Re < 100$)

Zusammenfassung—Es wurden die Konzentrationsprofile von Naphthalin-Dampf in einer Luftströmung durch Festbetten ausgemessen. Die Festbetten bestanden aus Naphthalinkugeln, welche in eine Matrix aus inerten Styrol-Divinylbenzol-Kopolymer-Perlen eingebettet waren. Diese Profile erlaubten die Bestimmung der tatsächlichen, treibenden Kräfte $(\Delta p)_a$, aus welchen die entsprechenden tatsächlichen Stoffübergangskoeffizienten ermittelt wurden. Der Festbettreaktor besaß einen Durchmesser von 6,59 cm, die Partikeldurchmesser variierten von 0,02480 cm bis 0,2000 cm. In der doppeltlogarithmischen Darstellung des j_d-Faktors über der Reynolds-Zahl ergab sich eine Gerade, welche im untersuchten Bereich ($0{,}1 < Re < 100$) durch die Gleichung $j_d = 1{,}33/Re^{0,4}$ wiedergegeben werden kann. Diese Berechnung, welche sowohl axiale wie radiale Beiträge erfaßt, unterscheidet sich von denen früherer Untersuchungen, in welchen die mittlere logarithmische treibende Kraft $(\Delta p)_m$ Verwendung fand. Das Ergebnis dieser Untersuchung wurde auf das Modell der Reihenschaltung von Apparaten angewandt und es wurde die Abhängigkeit der Peclet-Zahl von der Reynolds-Zahl ermittelt, welche zur Aufstellung des tatsächlichen Mischungsfaktors $F = (\Delta p)_a/(\Delta p)_m$ erforderlich ist.

ОПРЕДЕЛЕНИЕ КОЭФФИЦИЕНТОВ ТЕПЛООБМЕНА ПО ДВИЖУЩИМ СИЛАМ ДЛЯ ПОТОКА ГАЗОВ, ПРОТЕКАЮЩЕГО ЧЕРЕЗ ПЛОТНЫЕ СЛОИ ($0{,}1 < Pe < 100$)

Аннотация — В потоке воздуха, протекающем через плотные слои нафталиновых сфер, диспергированных в матрице инертных шариков сополимера дивинилбензола, измерялись профили концентрации паров нафталина. Эти профили позволили найти средние истинные движущие силы $(\Delta p)_a$ для определения соответствующих истинных коэффициентов теплообмена. В реакторе, диаметром 6,59 см, использовались частицы диаметром от 0,02480 до 0,2000 см. График зависимости j_d — коэффициента от чилса Рейнольдса, полученный по данным настоящего исследования, является линейным в логарифмических координатах, что для исследованного диапазона можно выразить в виде уравнения $j_d = 1{,}33/Pe^{0{,}40}$. Это соотношение, включающее осевую и радиальную дисперсию, отличается от ранее известной логарифмической осредненной движущей силы $(\Delta p)_m$. На основании полученных результатов была предложена модель, представляющая собой цепочку последовательно соединенных резервуаров, необходимая для определения истинного коэффициента смешения $f = (\Delta p)_a/(\Delta p)_m$.